Journal of Operation and Automation in Power Engineering

Vol. XX, No. XX, Dec. XXXX, Pages: XXXX (Proofed)

http://joape.uma.ac.ir

Research Paper

Energy Management of the Distribution Network Considering Electric Vehicles Connected to the Grid

Misagh Hedayati and *Ali Ghasemi-Marzbali* *

Department of Electrical and Biomedical Engineering, Mazandaran University of Science and Technology, Babol, Iran.

Abstract— *Given the growing trend in the electric vehicle industry and the increasing use of electric vehicles (EVs), the management and control of EV charging in electric distribution networks are becoming crucial. The widespread presence of electric vehicles has led to an increased load on the distribution network. This increase in electrical load can cause problems during peak hours and in specific network locations. To prevent these issues and improve the efficiency of the power grid, controlling the charging of electric vehicles is essential. By utilizing electric vehicle charging management systems, it is possible to intelligently control vehicle charging during times of lower electrical demand on the grid. These systems can initiate EV charging when the grid load is low and suspend it during peak load periods. This improvement in electric vehicle charging scheduling contributes to enhanced power grid efficiency and reduces issues related to electrical load. In this article, the charging and discharging management of electric vehicles in a standard sample microgrid, considering a load response program, is analyzed. The CPLEX solver in MATLAB is used for solving the optimization problem. To achieve this, an appropriate objective function is defined based on the load response program in the microgrid. Then, using the proposed CPLEX approach and considering operational constraints, optimal energy management of the microgrid is performed. Simulation results indicate that without proper planning for electric vehicle charging in the microgrid, the utilization of the microgrid leads to an 18% increase in costs.*

Keywords—Consumption management, network-connected vehicles, distribution network, optimization.

1. Introduction

Over the past two decades, substantial progress has been achieved in the development of electric vehicles (EVs), particularly in advanced transportation systems. Major automobile manufacturers are increasingly investing in large-scale EV production [1]. Rechargeable batteries, as the core components of EVs, not only supply the vehicles' energy requirements but also provide a viable method of electrical energy storage [2]. Although the storage capacity of a single vehicle is limited compared with power plants or grid-scale storage, the large number of EVs offers considerable potential for distributed energy storage. Effective scheduling of charging and discharging can therefore enhance EV utilization and enable energy exchange with the power grid [3]. The deployment of EVs also supports environmental objectives by reducing fossil fuel dependence and greenhouse gas emissions, thereby mitigating climate change and improving urban air quality [4]. Moreover, EVs represent an innovative technological trajectory in the automotive industry, with the potential to accelerate future advancements in sustainable transportation [5]. Smart management systems are essential for coordinating EV charging and discharging. These systems employ advanced algorithms and real-time data to align charging schedules with grid requirements, electricity prices, and renewable energy availability [6]. For instance, charging can be shifted to off-peak periods to alleviate demand during peak hours, improve grid efficiency, and reduce operational costs. By integrating information on battery status, vehicle availability, and network conditions, smart management systems enable more accurate and efficient scheduling [7]. In this study, a management framework for EV charging and discharging within a standard microgrid is developed. The model incorporates a demand response program, and the optimization problem is solved using the CPLEX method.

Graphical abstract

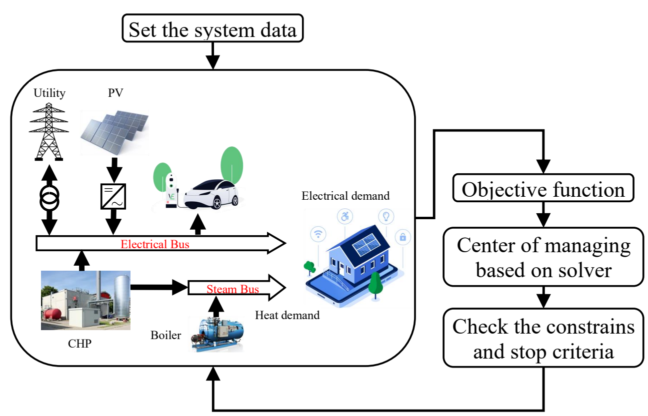

Received: 31 Dec. 2024
Revised: 14 Sept. 2025
Accepted: 22 Sept. 2025
*Corresponding author:
E-mail: ali.ghasemi@ustmb.ac.ir (A. Ghasemi-Marzbali)
DOI: 10.22098/joape.2025.16473.2271

1.1. Literature review

In recent years, numerous research studies have been conducted in the field of energy management. The following provides an overview of some of these studies. In Ref. [8], the effects of electric vehicle (EV) charging on the urban distribution network are evaluated using various charging strategies and penetration levels. The study examines charging during specific hours without considering the behavioral habits of EV owners. An intelligent load management system for controlling the charging of hybrid electric vehicles in residential networks is presented in [9]. The controlled and uncontrolled charging effects on the distribution system are investigated. A comprehensive network design model is utilized in [10] to calculate the required capital for a network influenced by various EV penetration levels. The assumption made is that a high percentage of these vehicles charge during off-peak hours. Ref. [11] investigates the impact of different EV penetration levels on aging transformers and feeder losses. Various researchers adopt different assumptions for EV battery sizing. For example, in [12] assumed continuous battery capacity ranging between 6 to 24 kilowatt-hours as a random variable, without providing a specific rationale for this selection. Additionally, determining the State of Charge (SOC) and the energy required for a full battery charge depends on factors such as daily travel distance, vehicle type, All-Electric Range (AER), and different vehicle operating modes.

In the realm of energy management in parking lots within microgrids, in [13] proposed an energy management system using fuzzy logic to optimize microgrid load profiles. In [14] introduced a multi-objective algorithm for energy management that aims to reduce operating costs and pollution. The algorithm determines the charging and discharging of EV batteries using fuzzy logic. Furthermore, artificial neural network methods are employed to estimate the production and load values of distributed energy resources. In [15] presented a decentralized multi-agent system for the optimal utilization of parking lots and distributed generation resources in a microgrid. This approach aims to balance power, improve system reliability, and distribute load optimally. In [16] addressed the management of parking charging and discharging in microgrids, considering the load response program and distributed storage. The goal is to reduce peak load and customer energy costs. Using a game theory-based approach, in [17] explored energy management and power sharing among electric vehicles in a parking lot. The study optimizes charging and discharging during specific time intervals, with the objective of maximizing energy efficiency. In [18], a method is proposed to engage bottom-line loads in energy management using an artificial intelligence system called Demand Response (DR). This method uses variable electricity prices or incentive policies to encourage consumers to adopt appropriate load patterns.

In [19], an energy balance strategy for plug-in hybrid electric vehicles (PHEVs) in microgrids is proposed, considering the coupling of information, power, and traffic networks (IN-PG-TN). A PHEV interaction model is built based on charging/discharging behavior and traffic mobility, leading to a spatiotemporal scheduling framework. On this basis, a two-layer deep deterministic policy gradient (DDPG) model is developed, where the upper layer minimizes microgrid costs and the lower layer optimizes PHEV energy management. In [20], an IoT-based Energy Management System (EMS) for Smart Microgrids is proposed to lower operational costs and EV owners' expenses. The system enables EV charging in residential microgrids and discharging in office microgrids, coordinated through Time-of-Use pricing. Optimal scheduling is achieved using the Pelican optimization algorithm while considering renewable integration, network limits, and EV requirements. In [21], an efficient energy management model for EV parking lots (EVPLs) is presented, enabling market participation and vehicle-to-grid (V2G) services to enhance profitability for both EVPLs and EV owners. The model treats EVPLs as distributed resources powered by renewables, operating in day-ahead and real-time markets while accounting for battery degradation, charging nonlinearity, and V2G incentives. Formulated as a mixed-integer linear program (MILP) and incorporating uncertainties via Monte Carlo Simulation, the approach ensures optimal profit under realistic conditions.

In [22], the integration of electric vehicles (EVs) into microgrids is addressed using vehicle-to-grid (V2G) technology to enhance sustainability and reduce costs. Uncertainties from EV demand, renewable generation, load variation, and market prices are modeled through the unscented transform, while a constrained optimization framework minimizes microgrid operating costs. To solve this, a modified marine predators algorithm (MMPA) is applied for efficient operation scheduling. In [23], a low-carbon planning approach for flexible distribution networks is proposed to address the challenges posed by distributed renewable energy and electric vehicles under the "dual carbon" goal. An aggregated dynamic model of EV charging and discharging boundaries is developed, and a two-layer planning framework is established using carbon emission flow theory. The upper layer focuses on network infrastructure, while the lower layer optimizes EV scheduling and user strategies to minimize costs. The model is further reformulated into a solvable mixed-integer second-order cone program. Therefore, Table 1 listed a comparative analysis of literature in EV and microgrid energy management.

1.2. Contributions and novelties

The management of electric vehicle (EV) charging and discharging in microgrids plays a pivotal role in balancing demand and supply within power transmission and distribution systems. With the rapid growth in EV adoption, unmanaged charging can significantly increase peak loads, strain generation and distribution capacity, and reduce overall system efficiency. Intelligent charging and discharging strategies can distribute demand more evenly, aligning consumption with periods of abundant generation—such as peak sunlight hours in photovoltaic systems—thereby maximizing the utilization of locally generated energy. By treating EVs as flexible, bidirectional storage assets, stored energy can be returned to the grid during periods of high demand, enhancing operational flexibility, maintaining supply–demand balance, and reducing reliance on costly peaking generation. In addition to improving energy efficiency, such coordinated management can lower operational costs across generation, distribution, and consumption stages. While recent research on microgrid energy management has employed various optimization techniques, including heuristic algorithms and commercial solvers, many studies address distributed generation, storage, and EVs separately or under simplified assumptions regarding user participation, renewable variability, and multi-energy integration. To address these gaps, this study proposes a unified optimization framework that integrates incentive-aware vehicle-to-grid (V2G) participation, joint electrical–thermal scheduling, and a two-stage operational strategy to enhance both economic and technical performance under uncertainty. The main contributions and novelties can be summarized as follows:

1) **Integrated electrical–thermal–V2G coordination:** simultaneous optimization of photovoltaic generation, combined heat and power (CHP) units, boilers, grid exchanges, and an aggregated EV fleet, with CHP modeled through coupled electricity–heat output characteristics.
2) **Endogenous incentive design for EV participation:** monetary rewards for EV owners are treated as decision variables, enabling the operator to balance economic gains, user engagement, and system stability within one model.
3) **Two-stage operational structure:** scenario-based day-ahead scheduling under renewable and behavioral uncertainty, followed by real-time re-optimization with explicit penalties for deviations.
4) **Realistic fleet-level EV modeling:** explicit representation of arrival/departure patterns, charging/discharging rates, state-

Table 1. Comparative analysis of literature in EV and microgrid energy management.

Ref	Focus area	Advantages	Disadvantages
[8]	EV charging impact on urban distribution network	Considers multiple strategies and penetration levels	Ignores behavioral habits of EV owners
[9]	Load management for hybrid EVs in residential networks	Analyzes both controlled and uncontrolled charging	Limited to residential networks, not scalable to large systems
[10]	Network design under EV penetration	Helps estimate capital requirements	Assumes most vehicles charge off-peak, which may not hold in practice
[11]	Transformer aging and feeder losses	Evaluates long-term network asset degradation	Does not account for smart management strategies
[12]	EV battery capacity assumptions	Considers uncertainty in battery size	Lacks justification for assumed range
[13]	Energy management in parking lots	Smooths load profile, intuitive method	Limited precision compared to advanced AI methods
[14]	Multi-objective EV management	Reduces costs and pollution, integrates renewables	Computationally complex; depends on accurate ANN training
[15]	Decentralized parking lot and distributed generation	Enhances balance and autonomy, scalable	Coordination complexity, high communication needs
[16]	Parking lot charging/discharging with DR	Reduces peak load and customer costs	Effectiveness depends on accurate demand response
[17]	EV energy sharing in parking lots	Optimizes charging/discharging collaboratively	Complex model, may be hard to implement in real systems
[18]	Demand Response (DR) with AI	Encourages better consumption patterns	Relies on consumer compliance and policy support
[19]	PHEVs in microgrids with traffic–energy coupling	Accounts for mobility + energy + information networks	Very complex, requires high data availability
[20]	IoT-based EMS for smart microgrids	Supports ToU pricing, integrates renewable energy	IoT-based systems vulnerable to cybersecurity risks
[21]	EV parking lots as market participants	Accounts for V2G, degradation, and real market dynamics	High modeling and computation complexity
[22]	EV–microgrid integration with V2G	Efficient handling of uncertainty, cost reduction	Metaheuristic solutions may not guarantee global optimum
[23]	Low-carbon planning for EV + renewables	Aligns with "dual carbon" goals, holistic approach	Requires advanced infrastructure and large-scale data

of-charge constraints, and heterogeneous user willingness to participate in V2G.

5) **Optimal mixed-integer formulation and benchmarking:** problem implementation in MATLAB with CPLEX ensures reproducible, provably optimal schedules, providing a benchmark for alternative solution methods.

1.3. Paper structure

The article is organized into the following sections. In the Section 2, the problem is modeled, along with the relevant mathematics, which are presented in detail. The Section 3 includes simulation results and numerical analyses. In the Section 4, conclusions are drawn, and recommendations for future work are provided.

2. Problem Modeling

This section presents the complete modeling and scheduling framework developed in the study. The proposed approach begins with the characterization of all system components, including photovoltaic generation, combined heat and power units, boilers, electrical and thermal storage devices, and electric vehicle charging/discharging stations. Each component is represented through mathematical models that capture operational limits, efficiencies, and energy conversion relationships. These models are integrated into a mixed-integer linear programming (MILP) formulation designed to coordinate day-ahead scheduling with real-time adjustments under renewable generation and demand uncertainty. The scheduling process consists of three main steps: (1) scenario generation for uncertain variables such as PV output and EV arrival state-of-charge; (2) day-ahead optimization to determine unit commitment, charging/discharging plans, and energy exchanges; and (3) real-time re-optimization to adjust setpoints based on updated system states, ensuring reliability and economic efficiency. The objective function minimizes total operating cost while respecting energy balance, operational constraints, and user participation requirements.

2.1. Vehicle-to-Grid (V2G) technology

V2G technology is an innovative concept in the realm of electric vehicles that refers to the bidirectional nature of the connection between electric vehicles and the power grid. This technology enables electric vehicles to act as dynamic and interactive energy sources for the power grid. In V2G technology, electric vehicles can both draw electricity from the power grid and feed energy back into it. This means that electric vehicles can not only utilize the power grid to charge their batteries but, during times of high demand on the power grid, they can return the stored energy in their batteries to the grid and function as an energy supply source for the national power system [24]. Fig. 1 illustrates V2G technology.

In addition to charging and discharging stations, other infrastructures are essential for the success of V2G. These infrastructures are related to communication requirements and data acquisition in artificial intelligence networks. To optimally utilize V2G and manage the charging and discharging of vehicles, artificial intelligence networks are crucial. For this purpose, artificial intelligence-based measurements and telecommunication systems are required. These telecommunication systems in artificial intelligence networks can be implemented either through wired or wireless connections. Since electric vehicles are, in a way, idle capital resources during parking times and may incur costs for owners from an economic perspective (such as parking and maintenance costs), the concept of V2G has been designed as a

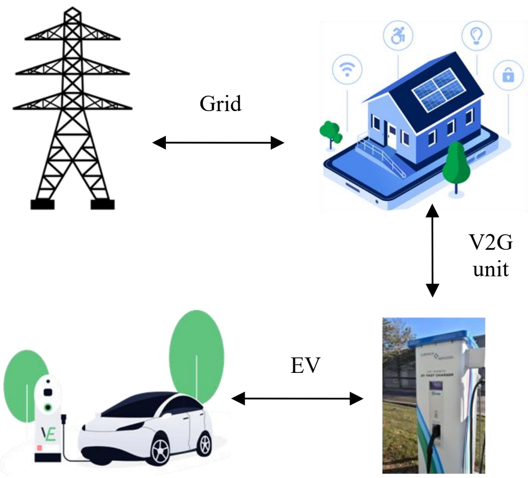

Fig. 1. Vehicle-to-grid (V2G) technology.

solution to leverage these underutilized resources. Each V2G unit has a converter and a battery, and the internal structure of V2G can be illustrated as shown in Fig. 2.

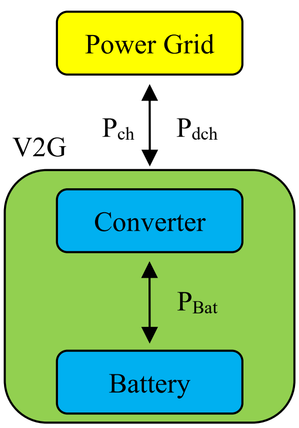

Fig. 2. Internal structure of V2G technology.

The transferable power (P_{Bat}) to or from the converter in the V2G system can vary. Considering the battery efficiency and power transmission efficiency, the power exchange capability of V2G with the network is defined by the following equation:

$$P_{Ch} = \frac{P_{Bat}}{\eta c} \tag{1}$$

$$P_{dch} = P_{Bat} \times \eta d \tag{2}$$

The above relationships indicate that if ηd and ηc are not unitary, V2G must purchase more power than it stores to charge its battery. Meanwhile, the power delivered to the grid is less than the stored battery power. Therefore, the closer ηd and ηc are to unity, the V2G owner obtains more profit by utilizing the battery capacity efficiently.

2.2. Problem objective function

The considered objective function aims at reducing the operating costs of the microgrid. The proposed cost function is a combination of purchased energy from the upper-level network, the cost of distributed generation resources, and the cost of electric vehicle parking, and is expressed by the following Eq. (3) [25]:

$$f_1 = E_{Cost} + H_{Cost} \tag{3}$$

The cost of requested electrical energy is calculated using Eq. (4). This cost function is a combination of the cost of purchased power from the national grid, CHP operation costs, loss costs, and electric vehicle parking costs. Significant reductions in power consumption during peak hours can have a notable impact on lowering operating costs:

$$E_{Cost} = \sum_{t=1}^{24} C_{NG}(t) + C_{PV}(t) + + C_{CHP-E}(t) + C_{PL}(t) \tag{4}$$

where, C_{NG}, C_{PV}, C_{CHP-E}, and C_{PL} represent the cost of purchased power from the national grid, the cost of decentralized photovoltaic power generation, the cost of electric power produced by the CHP unit, and the parking cost during the time interval 't', respectively. In this research, the value of 't' is considered equal to one hour, and consequently, the planning period is the same as the production planning, which is 24 hours. T represents the total number of hours (T = 1, 2, ..., 24). The cost of purchasing energy from the national grid is calculated using the Eq. (5):

$$C_{NG}(t) = \Gamma(t) \times P_{NG}(t) \tag{5}$$

where, $P_{NG}(t)$ represents the exchanged power with the national grid during period 't', and $\Gamma(t)$ is the cost per kilowatt-hour of energy in the market. The costs of decentralized photovoltaic and CHP production are calculated by the following relationships:

$$C_{PV}(t) = \sigma_{PV} \times P_{PV}(t) \tag{6}$$

$$C_{CHP-E}(t) = \sigma_{CHP} \times P_{CHP}(t) \tag{7}$$

where, $P_{PV}(t)$ and $P_{CHP}(t)$ represent the generated power by photovoltaic and electrical power by CHP unit, respectively. σ_{PV} and σ_{CHP} are the coefficients of power generation cost for these sources. The parking cost is calculated using the Eq. (8):

$$C_{PL}(t) = \vartheta(t) \times (P_{Ch}(t) + P_{dCh}(t)) \tag{8}$$

where, $P_{Ch}(t)$ and $P_{dCh}(t)$ represent the input and output powers of the parking lot, and $\vartheta(t)$ is the cost of each kilowatt-hour of exchanged electricity in the electric vehicle parking lot during hour t. The cost of thermal energy is calculated according to Eq. (9) [26]:

$$H_{Cost} = \sum_{t=1}^{24} C_{HO}(t) + C_{CHP-H}(t) \tag{9}$$

where, the cost of thermal unit of CHP unit $C_{CHP-H}(t)$, and the cost of the boiler $C_{HO}(t)$ are represented. The cost per unit of thermal energy for the boiler is calculated using Eq. (10):

$$C_{HO}(t) = C_{HO-F}(t) + C_{HO-SC}(t) \tag{10}$$

where, the cost of fuel consumption $C_{HO-F}(t)$, and the cost of turning on/off this unit $C_{HO-SC}(t)$ are represented. The fuel cost is also calculated using Eq. (11):

$$C_{HO}(t) = \alpha_{HO} H^2(t) + \beta_{HO} H(t) + \delta_{HO} \tag{11}$$

where, $H(t)$ represents the amount of heat produced by the boiler, and α_{HO}, β_{HO} and δ_{HO} are the coefficients of the boiler cost. The cost of turning on/off this unit is also obtained using Eq. (12):

$$C_{HO}(t) = SUC \times |(U(t) - U(t-1)| \tag{12}$$

The cost of heat production by the CHP unit is given by Eq. (14):

$$C_{CHP-H}(t) = \tau_{CHP} \times H_{CHP}(t) \tag{13}$$

where, $H_{CHP}(t)$ represents the amount of heat produced by the CHP unit, and τ_{CHP} is the cost per kilowatt of heat produced by this unit.

2.3. Operational constraints

To make the optimization model and its assumptions fully transparent, the primary hourly constraints (previously referenced as Eqs. (14)–(21)) are stated here in explicit form and each constraint is accompanied by a short rationale [27]. The model uses a 24-hour horizon with hourly time steps ($\Delta t = 1\,h$). Index t denotes the hour. Let, $P_{PV}(t)$ — photovoltaic power delivered to the AC bus at hour $t(kW)$. $P^{E}_{CHP}(t)$ — electric and thermal output of the CHP unit at hour $t(kW)$. $Q_{boiler}(t)$ — thermal output of the boiler at hour $t(kW)$. $P^{buy}_{grid}(t)$, $P^{sell}_{grid}(t)$ — power purchased from/sold to the upstream grid at hour $t(kW)$, both non-negative. $P^{ch}_{par}(t)$, $P^{dis}_{par}(t)$ — aggregate charging and discharging (V2G) power of the parking lot at hour $t(kW)$. $N_{present}(t)$ — number of vehicles connected in the parking lot during hour t (integer, estimated or observed). P^{max}_{ch}, P^{max}_{dis} — per-vehicle maximum charging and discharging power (kW). E_{batt} — per-vehicle usable battery energy capacity (kWh). $SOC_i(t)$ — state of charge of vehicle i at hour t (fraction, 0–1). $P_{load}(t)$, $Q_{load}(t)$ — electrical and thermal demand at hour $t(kW)$. All numeric parameter values used in the case study are taken from the microgrid description (50-vehicle parking lot; 90 kWh battery capacity; per-vehicle charge/discharge limit 8 kW; SOC upper bound 95%; PV nominal 150 kW; CHP nominal 100 kW electric/120 kW thermal; boiler 120 kW).

Electric power balance (hourly):

$$\begin{aligned} &P_{\mathrm{PV}}(t) + P^{E}_{\mathrm{CHP}}(t) + P^{\mathrm{buy}}_{\mathrm{grid}}(t) + P^{\mathrm{dis}}_{\mathrm{par}}(t) = \\ &P_{\mathrm{load}}(t) + P^{\mathrm{ch}}_{\mathrm{par}}(t) + P^{\mathrm{sell}}_{\mathrm{grid}}(t) + P_{\mathrm{loss}}(t), \quad \forall t \end{aligned} \tag{14}$$

Thermal power balance (hourly):

$$Q_{\mathrm{CHP}}(t) + Q_{\mathrm{boiler}}(t) = Q_{\mathrm{load}}(t) + Q^{\mathrm{th}}_{\mathrm{loss}}(t), \quad \forall t \tag{15}$$

Grid exchange limits (hourly):

$$\begin{aligned} &0 \le P^{\mathrm{buy}}_{\mathrm{grid}}(t) \le P^{(\mathrm{buy,max})}_{\mathrm{grid}}, \\ &0 \le P^{\mathrm{sell}}_{\mathrm{grid}}(t) \le P^{(\mathrm{sell,max})}_{\mathrm{grid}}, \quad \forall t \end{aligned} \tag{16}$$

CHP unit technical limits and coupling (hourly):
On/off and capacity bounds:

$$P^{(E,\min)}_{\mathrm{CHP}}\, u_{\mathrm{CHP}}(t) \le P^{E}_{\mathrm{CHP}}(t) \le P^{(E,\max)}_{\mathrm{CHP}}\, u_{\mathrm{CHP}}(t) \tag{17}$$

$$Q^{\min}_{\mathrm{CHP}}\, u_{\mathrm{CHP}}(t) \le Q_{\mathrm{CHP}}(t) \le Q^{\max}_{\mathrm{CHP}}\, u_{\mathrm{CHP}}(t) \tag{18}$$

Coupling (capability curve linearized as convex constraints):

$$\begin{aligned} &\sum_{k=1}^{K} \lambda_k(t)\, P^{(E,k)}_{\mathrm{CHP}} = P^{E}_{\mathrm{CHP}}(t), \quad \sum_{k=1}^{K} \lambda_k(t)\, Q^{k}_{\mathrm{CHP}} = Q_{\mathrm{CHP}}(t), \\ &\sum_{k=1}^{K} \lambda_k(t) = u_{\mathrm{CHP}}(t), \quad \lambda_k(t) \ge 0 \end{aligned} \tag{19}$$

Where, (i) $u_{\mathrm{CHP}}(t) \in \{0,1\}$ is the on/off status that links start/stop costs to operation (the cost expressions in Eq. (12) are applied when u_{CHP} changes). (ii) the CHP capability ("power capability curve", Fig. 3) is enforced by a standard convex (piecewise-linear) representation: the continuous outputs P^{E}_{CHP} and Q_{CHP} are represented as convex combinations of a small set K of vertices that lie on the manufacturer capability curve (this preserves linearity for the MILP). The studied microgrid uses nominal bounds $P^{E,\max}_{\mathrm{CHP}} = 100$ kW, $Q^{\max}_{\mathrm{CHP}} = 120$ kW, as reported in the case description.

Let $u_t \in \{0,1\}$ denote the CHP on/off status at hour t, while P^{CHP}_t and Q^{CHP}_t denote the CHP electric and thermal outputs at hour $t(kW)$, as defined previously. To capture realistic dynamic behaviour of the CHP unit and to keep the formulation linear, the following standard linear constraints are introduced: start-up/shutdown linking, ramp-rate limits (electrical side), and minimum up/down time constraints. These constraints are formulated so that they integrate directly with the MILP structure already employed (piecewise-linear capability curve and on/off binaries).

Startup/shutdown indicators: Introduce binary variables v_t (start-up at hour t) and z_t (shutdown at hour t), linked to the on/off status:

$$\mathrm{v}_t - \mathrm{z}_t = \mathrm{u}_t - \mathrm{u}_{t-1} \tag{20}$$

$$v_t + z_t \le 1 \tag{21}$$

Ramp-rate limits (electrical output):

Ramping is enforced on the electrical output P^{CHP}_t. The formulation below permits normal (within-online) ramping and allows the unit to move from zero to a feasible operating point when starting, without introducing nonlinearities:

$$P^{\mathrm{CHP}}_t - P^{\mathrm{CHP}}_{t-1} \le R^{\mathrm{CHP}}_{\mathrm{up}}\, u_{t-1} + P^{\mathrm{CHP}}_{\max}\, v_t, \quad \forall t \tag{22}$$

$$P^{\mathrm{CHP}}_{t-1} - P^{\mathrm{CHP}}_t \le R^{\mathrm{CHP}}_{\mathrm{down}}\, u_t + P^{\mathrm{CHP}}_{\max}\, z_t, \quad \forall t \tag{23}$$

Here $R^{\mathrm{CHP}}_{\mathrm{up}}$ and $R^{\mathrm{CHP}}_{\mathrm{down}}$ are the hourly ramp-up and ramp-down limits ($\mathrm{kW} \cdot \mathrm{h}^{-1}$), respectively, and $P^{\mathrm{CHP}}_{\max}$ is the nominal electrical rating. The additive $P^{\mathrm{CHP}}_{\max}$ terms multiplied by the start-up/shutdown indicators allow the model to reach any feasible operating point immediately after a start (this is a conservative, standard linear device that avoids infeasibility at the moment of start) [28]. The capability curve coupling (Eq. (19)) still enforces simultaneous feasible thermal/electrical combinations; therefore, thermal changes are implicitly constrained by the same device physics. If a separate explicit thermal ramp constraint is desired, it can be added analogously on Q^{CHP}_t.

Minimum up/minimum down times: To prevent unrealistically frequent cycling, minimum up time UT and minimum down time DT constraints are imposed using the start/shutdown indicators:

$$\sum_{k=t}^{t+UT-1} u_k \ge UT \cdot v_t, \quad \forall t = 1, \ldots, T - UT + 1 \tag{24}$$

$$\sum_{k=t}^{t+DT-1} (1-u_k) \geq DT \cdot z_t, \qquad \forall t = 1, \ldots, T-DT+1 \quad (25)$$

These linear constraints force the unit to remain ON for at least UT consecutive hours after a start, and OFF for at least DT consecutive hours after a shutdown. The power capability curve of a CHP unit is illustrated in Fig. 3.

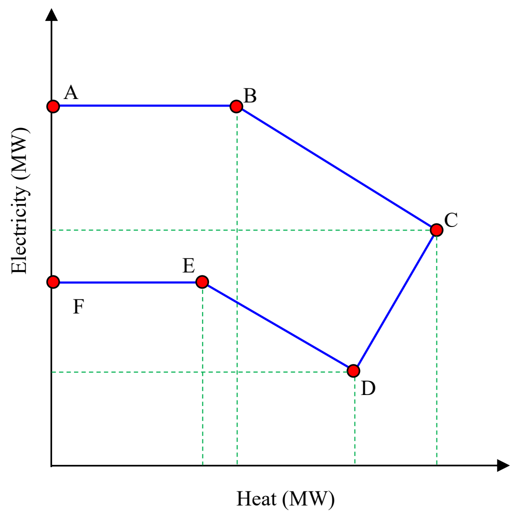

Fig. 3. Power capability curve of CHP unit.

Boiler capacity (hourly):

$$0 \leq Q_{\text{boiler}}(t) \leq Q_{\text{boiler}}^{\max}, \qquad \forall t \quad (26)$$

Where, $Q_{boiler}^{max} = 120kW$ the studied case.
Parking lot (EV) charge/discharge limits (hourly, aggregated):

$$\begin{aligned} &0 \leq P_{\text{par}}^{\text{ch}}(t) \leq N_{\text{present}}(t)\, P_{\text{ch}}^{\max}, \\ &0 \leq P_{\text{par}}^{\text{dis}}(t) \leq N_{\text{present}}(t)\, P_{\text{dis}}^{\max}, \qquad \forall t \end{aligned} \quad (27)$$

with $P_{\text{ch}}^{\max} = P_{\text{dis}}^{\max} = 8$ kW per vehicle and $N_{\text{present}}(t) \leq 50$ (parking lot capacity). Using an aggregated formulation keeps the model compact and links limits directly to the observed/forecast number of connected vehicles.

State of charge (SOC) dynamics and SOC bounds (hourly, per vehicle i or aggregated): Per-vehicle dynamics (preferred for accuracy, aggregated if privacy/performance is desired):

$$\begin{aligned} &SOC_i(t+1) = \\ &SOC_i(t) + \left(\eta_{\text{ch}} P_{\text{EV},i}^{\text{ch}}(t) - \frac{P_{\text{EV},i}^{\text{dis}}(t)}{\eta_{\text{dis}}}\right) \frac{\Delta t}{E_{\text{batt},i}} \end{aligned} \quad (28)$$

$$SOC^{\min} \leq SOC_i(t) \leq SOC^{\max}, \qquad \forall i, t \quad (29)$$

Typical values used in the case study are $E_{\text{batt},i} = 90$ kWh (nominal battery capacity), $\text{SOC}^{\max} = 0.95$ (maximum allowed charge, chosen to reduce calendar/cycle degradation), and charging/discharging efficiencies η_{ch} and η_{dis}, assumed near typical values (e.g., 0.90–0.95). The time interval Δt is equal to 1 hour.

Aggregation is performed by summing energy increment terms when an aggregate SOC state is used. Let τ_i^{arr} and τ_i^{dep} denote the arrival and departure times of vehicle i, and $\text{SOC}_{i,\tau_i^{\text{arr}}}^{\text{init}}$ be its initial state of charge (SoC) upon arrival. Vehicles departing within the scheduling horizon must satisfy:

$$SOC_{i,\tau_i^{\text{dep}}} \geq SOC_{i,\tau_i^{\text{arr}}}^{\text{init}} \quad (30)$$

This ensures that the energy level upon departure meets or exceeds the arrival level. To represent degradation without assigning a cost, a daily throughput cap is applied. Let $E_{i,t}^{\text{ch}} = P_{i,t}^{\text{ch}}\,\Delta t$ and $E_{i,t}^{\text{dch}} = P_{i,t}^{\text{dch}}\,\Delta t$ be the charging and discharging energies, respectively. The cumulative daily throughput THR_i for each vehicle is:

$$THR_i = \sum_t \left(E_{i,t}^{\text{ch}} + E_{i,t}^{\text{dch}}\right) \quad (31)$$

The throughput is limited by:

$$THR_i \leq \theta_i\, C_i, \qquad \forall i \quad (32)$$

where θ_i is the maximum allowable daily throughput factor. In the base case, $\theta_i = 2.0$ limits the total daily energy exchanged to twice the nominal capacity, corresponding to a maximum of two full equivalent cycles per day.

EV participation indicator and incentives: The operator's decision to offer a monetary reward to vehicle owners is modeled explicitly: for each vehicle i and hour t the binary indicator $y_i(t) \in \{0,1\}$ denotes whether the owner accepts managed charging; charging power is limited by $P_{\text{EV},i}^{\text{ch}}(t) \leq P_{\text{ch}}^{\max} \cdot y_i(t)$. The reward $r(t)$ appears in the objective function as an operator cost and is also constrained to feasible bounds (e.g.,$0 \leq r(t) \leq r_{\max}$, as described in Section 2.2. The manuscript already treats the reward as an operator decision variable and uses it to trade off operator profit and owner participation.

Linearization/convexification of non-linearities: The model is implemented as a mixed-integer linear program (MILP) by (i) piecewise-linear convexification of the CHP capability curve (Fig. 3) via vertex weights $\lambda_k(t)$, (ii) linearizing start/stop costs with on/off binaries $u_{\text{CHP}}(t)$, and (iii) treating PV scenarios as exogenous hourly upper bounds $P_{\text{PV}}^{\max}(t)$ for each scenario in the day-ahead stage. This MILP structure permits exact solution by an industrial solver while preserving the key physical constraints.

Stochastic → real-time structure: For day-ahead planning the model ingests scenario-based bounds for $P_{\text{PV}}^{\max}(t)$, $N_{\text{present}}(t)$, and initial SOC; real-time planning fixes realized $N_{\text{present}}(t)$ and $P_{\text{PV}}(t)$ and resolves the MILP with realized values while imposing deviation penalties (the case uses a penalty of 1 USD/kWh for forecast error).

The numerical choices used in the case study are motivated as follows. A parking lot capacity of 50 vehicles is representative of a medium-sized building installation and is used throughout the simulations; the per-vehicle nominal battery capacity is taken as 90 kWh (this reflects contemporary passenger BEV battery sizes used in the sensitivity study), and the per-vehicle maximum AC charging/discharging rate is 8 kW (a Level-2/low-power V2G bound commonly used in parking applications). To reduce calendar and cycle degradation, the maximum state-of-charge is capped at 95%. The distributed energy resource sizes used in the numerical example are a 150 kW PV array, a CHP rated at 100 kW electric/120 kW thermal, and a 120 kW boiler; production costs and the TOU exchange price profile follow the values and figures already reported in Section 3. These parameter values are taken directly from the case description and are used consistently in the scenario and real-time simulations. The incentive provided to each EV owner is expressed as an energy-based relation, linked to the managed charging or discharging schedule. For each vehicle i and time step t, the incentive amount is defined as:

$$E_{i,t}^{\text{inc}} = R_{i,t}\, P_{i,t}^{\text{ch}}\,\Delta t \quad (33)$$

where $R_{i,t}(kWh)$ is the incentive rate, $P^{\mathrm{ch}}_{i,t}(kW)$ is the scheduled charging power, and $\Delta t(h)$ is the time step length. Participation is enforced through the binary decision variable $\mathrm{z_{i,t}} \in \{0,1\}$:

$$0 \le P^{\mathrm{ch}}_{i,t} \le z_{i,t}\, P^{\max}_{i}, \qquad \forall i,t \tag{34}$$

so that no charging is assigned when the vehicle declines participation ($\mathrm{z_{i,t}} = 0$). The real-time deviation penalty is represented by the absolute difference between actual and scheduled net power exchange with the grid. Non-negative deviation variables δ^{+}_{t} and δ^{-}_{t} linearize this difference:

$$P^{\mathrm{act}}_{t} - P^{\mathrm{sch}}_{t} = \delta^{+}_{t} - \delta^{-}_{t}, \qquad \forall t \tag{35}$$

$$\delta^{+}_{t} \ge 0, \qquad \delta^{-}_{t} \ge 0, \qquad \forall t \tag{36}$$

The magnitude of deviation is then:

$$\Delta P_t = \delta^{+}_{t} + \delta^{-}_{t}, \qquad \forall t \tag{37}$$

and the associated penalty energy for the period is:

$$E^{\mathrm{pen}}_{t} = \Delta P_t\, \Delta t, \qquad \forall t \tag{38}$$

2.4. The proposed framework

The proposed MILP model is implemented in MATLAB R2023a using the CPLEX 22.1 optimization solver. Simulations are executed on a desktop computer equipped with an Intel Core i7 processor (3.2 GHz) and 32 GB of RAM, running Windows 11 Pro (64-bit). The solver is configured with a relative MIP gap tolerance of 0.01, a maximum runtime limit of 3600 seconds per optimization stage, and default presolve and cut generation settings. Scenario generation and data preprocessing routines are coded in MATLAB, while post-processing of optimization results and graphical output are also performed within the same environment. The simulation workflow is modular, enabling straightforward adaptation to different system sizes, component characteristics, and pricing structures.

3. Simulation Results

In this study, optimal energy management planning in a residential building (BEMS) was carried out in two stages: first, next-day optimal planning, and second, real-time optimal planning. This approach was adopted to maximize the benefits of energy management in the studied system. In this way, if the predicted values in the next-day planning approach are close to the real-time values, the benefits of energy management in the microgrid are maximized. Otherwise, a penalty must be incurred. It is worth noting that the optimizations were performed over a 24-hour period with one-hour intervals, and the simulation results are presented in the following section.

3.1. Introduction of the studied microgrid

The microgrid chosen for simulation in this dissertation is an imaginary building with an electric vehicle parking lot with a capacity of 50 electric vehicles, capable of two-way electricity exchange with the distribution grid. In this study, the capacity of the electric vehicle parking lot is utilized for electricity storage and participation in Demand Response Programs (DRP). It is assumed that the battery capacity of the electric vehicle parking lot is 90 kWh, and the maximum charging and discharging rate for each vehicle is 8 kW [29]. It should be noted that, to prevent battery degradation, the maximum allowed state of charge (SOC) for vehicle batteries is set at SOC = 95%. The structure of the studied microgrid is illustrated in Fig. 4.

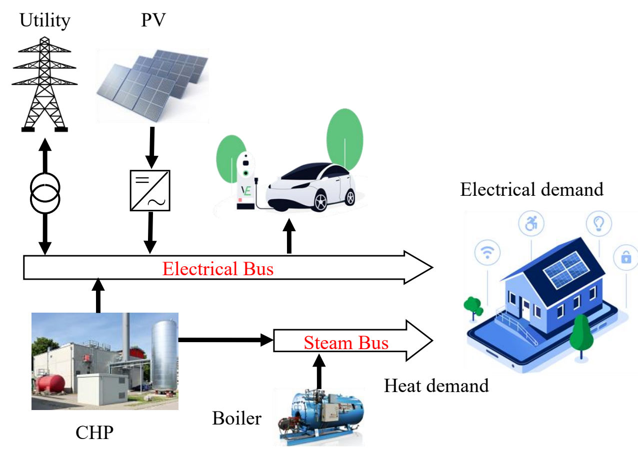

Fig. 4. Diagram of the studied microgrid.

In the studied microgrid, a photovoltaic (PV) array with a nominal power of 150 kW, along with a combined heat and power (CHP) unit with nominal electrical and thermal powers of 100 kW and 120 kW, respectively, and a boiler with a nominal power of 120 kW, are utilized. The cost of power production for the CHP unit is calculated at \$0.47 per kWh, and the cost of power production by the boiler is \$0.35 per kWh. It should be noted that the price of electric energy exchange in the microgrid is based on Time-of-Use (TOU) pricing, and the hourly energy prices are illustrated in Fig. 5. The parameters of this system are listed in Table 2.

Table 2. Summary of input data used in the case study.

Parameter	Value	Unit
PV array rated capacity	150	kW
CHP rated electric capacity	100	kW
CHP rated thermal capacity	120	kW
Boiler rated thermal capacity	120	kW
CHP electricity production cost	0.47	USD/kWh
Boiler heat production cost	0.35	USD/kWh
EV battery nominal capacity	90	kWh
EV charger power limit (per vehicle)	8	kW
Number of EVs (parking lot capacity)	50	–
Maximum allowed SOC	95	%
Time-of-use electricity price (peak/off-peak/valley)	0.21/0.14/0.08	USD/kWh
EV charging cost in parking lot	0.8	USD/kWh
Natural gas price	0.32	USD/m^3
PV scenario outputs (low/medium/high)	103/118/148	kW
EV arrival distribution	Mean 13.8, SD 4.6	vehicles
Initial SOC distribution	Variable (5 segments)	%
Daily throughput limit per EV	2× nominal capacity	kWh/day
Deviation penalty	1.0	USD/kWh

Continuing with Fig. 6, the values of electrical and thermal loads in the microgrid for the next day are displayed. The load values in this microgrid correspond to the energy consumption of typical building loads, such as heating and cooling systems, refrigerators, televisions, electronic devices, and other appliances.

Based on the chart in Fig. 6, the highest level of electrical consumption in the microgrid occurs at 20:00, reaching approximately 210 kWh. On the other hand, the highest thermal load consumption in the microgrid is around 132.7 kWh at 11:00. If there are differences between the predicted and actual load values, a penalty of \$1 per kWh difference is applied. The cost of charging electric vehicles in the parking lot is assumed to be \$0.8 per kWh. Additionally, if electric vehicles participate in the microgrid energy management programs, rewards are provided, leading to a reduction in charging costs for the vehicles in the parking lot and even generating income for the vehicle owners. Under these conditions, the microgrid energy management system

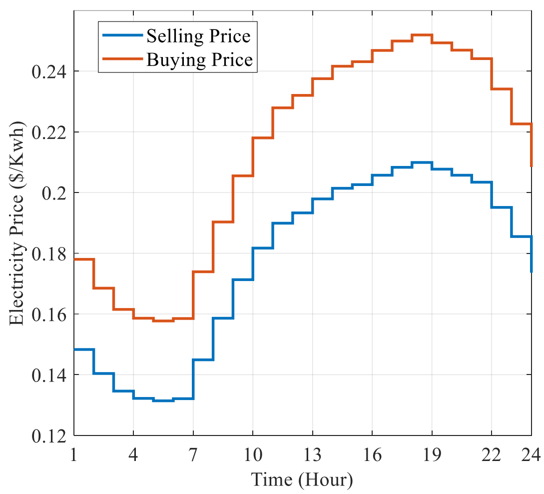

Fig. 5. Hourly values of exchanged electricity prices with the upstream grid.

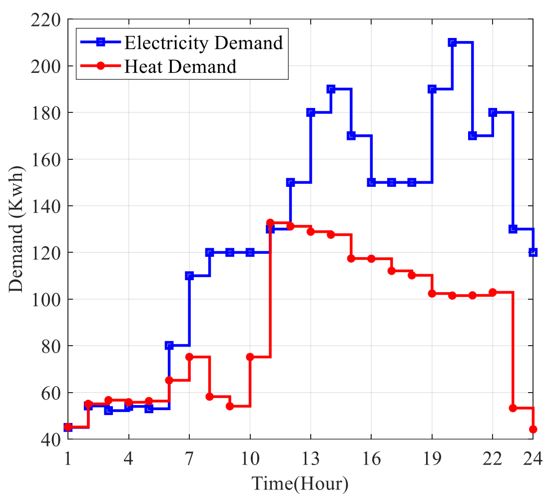

Fig. 6. Energy consumption values of loads in the microgrid.

must optimize energy management to maximize the utilization of electrical and thermal resources available in the microgrid, aiming to reduce energy supply costs. Next, the results of the optimization are analyzed.

3.2. Day-Ahead planning

For day-ahead planning in the microgrid, we required data such as solar radiation intensity, the generating capacity of the photovoltaic array, the presence status of electric vehicles in the parking lot, the battery charge level of vehicles, the amount of electrical and thermal loads, energy prices per hour, and operational constraints on resources. To estimate solar radiation intensity and, consequently, the generating capacity of photovoltaic resources, weather data for the study area was utilized, and the beta probability density function was employed to model solar radiation intensity. In this study, the beta probability density function coefficients for solar radiation intensity were assumed to be $\alpha = 2$ and $\beta = 5$. Using the beta probability density function for solar radiation intensity, three different scenarios for solar radiation intensity were selected, as shown in Fig. 7, and these data were employed during the simulation process.

Fig. 8 illustrates the estimated hourly parking status of electric vehicles (EVs) in the microgrid. In the left subplot, the total

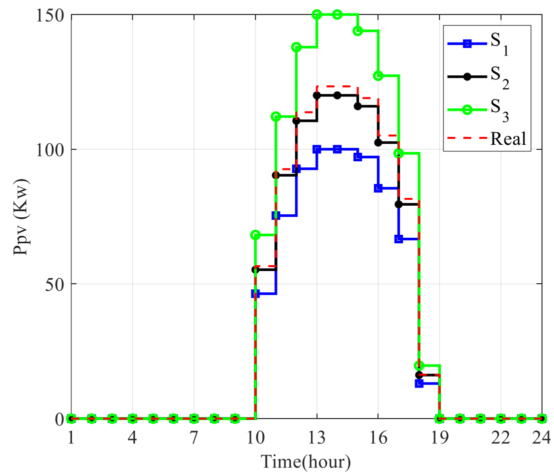

Fig. 7. Selected values for photovoltaic array generating capacity in three scenarios.

number of parked EVs per hour is obtained by summing the binary status variable (1= parked, 0= not parked) across the fleet. The number of vehicles present in the parking facility ranges from 0% of capacity (no vehicles connected) during early morning hours to a maximum of 12% of capacity (6 out of 50 EVs) during the busiest periods. The mean occupancy over the 24-hour horizon is approximately 3.2 vehicles, equivalent to 6.4% of total capacity, with a standard deviation of 1.85 vehicles (∼3.7% of capacity). This indicates relatively low and variable utilization of the parking facility, with occasional short-term clustering of arrivals. The right subplot presents a three-dimensional mesh surface showing the binary parking state of each vehicle over time. The visualization highlights significant heterogeneity in parking behavior: certain EVs remain connected for contiguous multi-hour periods, while others display isolated short-term stays. These occupancy patterns are critical for operational planning, as they determine the temporal availability of distributed storage capacity for vehicle-to-grid (V2G) services. When aligned with periods of high renewable generation, even modest occupancy levels can provide valuable load-shifting potential, reduce peak grid imports, and enhance the economic and technical performance of the microgrid.

The state of charge (SOC) in electric vehicle batteries is determined using factors such as distance traveled, battery type, and efficiency. However, these factors are not uniform for all electric vehicles, and the SOC levels in batteries can be considered as a random variable with a normal distribution. The initial SOC values for electric vehicles are illustrated based on the specified scenario in Fig. 9. The probability density function considered for the initial charge level of vehicles is divided into five segments.

Fig. 10 presents the initial state of charge (SOC) for 50 electric vehicles (EVs) upon arrival at the microgrid's parking facility. The SOC values range from a minimum of approximately 36.52% to a maximum of 78.26%, with most vehicles clustering between 60% and 75%. The fleet's mean initial SOC is around 60.7%, indicating that, on average, vehicles arrive with over half of their nominal battery capacity available. Such variability arises from differences in prior driving distances, operational patterns, and off-site charging availability. This distribution is a critical parameter for the microgrid's energy management system, as it affects aggregate charging requirements, vehicle-to-grid (V2G) discharge potential, and the formulation of optimal charging schedules. Accurately capturing these initial charge levels enables coordinated charging that can reduce peak demand, maximize use of local renewable generation, and enhance overall system efficiency.

Fig. 11 depicts the inverse slope of the performance curve for

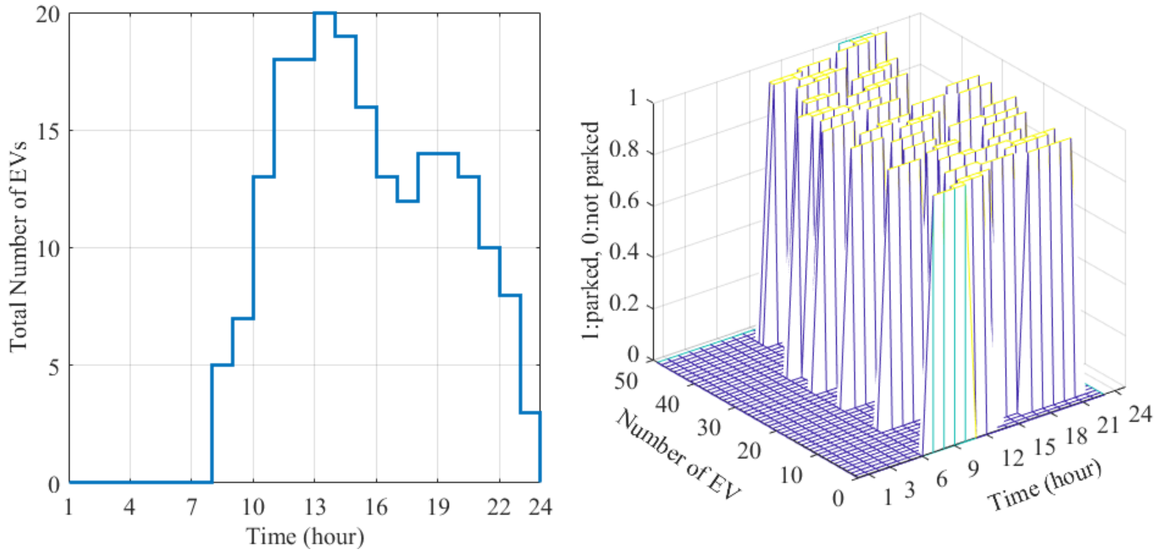

Fig. 8. Estimated number of electric vehicles in the parking lot for each hour.

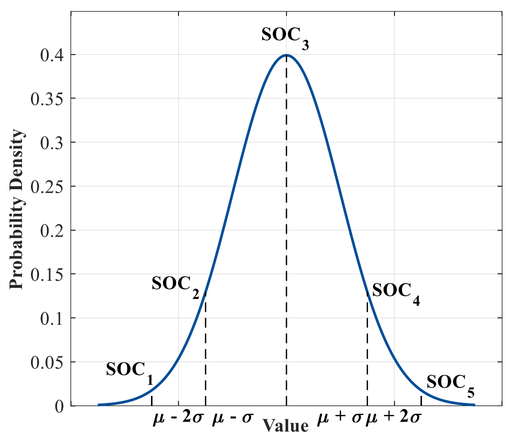

Fig. 9. Probability density function of initial charge level in electric vehicles.

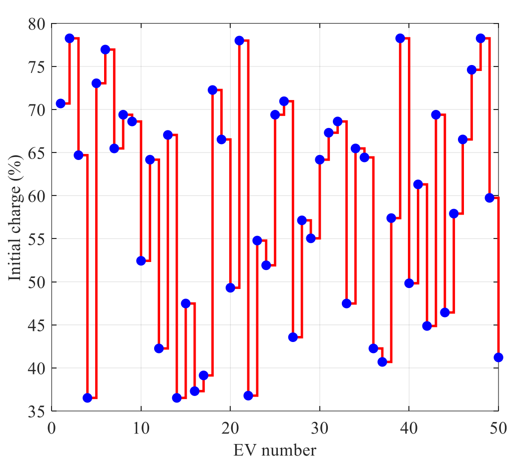

Fig. 10. Initial charge of electric vehicles in the microgrid.

50 EVs in the microgrid, representing each vehicle's response rate to monetary rewards within the energy management program. The measured values range from a minimum of 100 to a maximum of 200, with the majority falling between 120 and 180. The fleet's mean response rate is approximately 144.9, indicating a moderate average sensitivity to incentives. Higher values correspond to steeper performance curves, signifying greater willingness to adjust charging or discharging behavior in response to rewards, whereas lower values indicate reduced responsiveness. This parameter is essential for modeling incentive-based participation in coordinated charging strategies, as it directly influences the operator's ability to shape load profiles, optimize V2G contributions, and reduce peak demand in the microgrid.

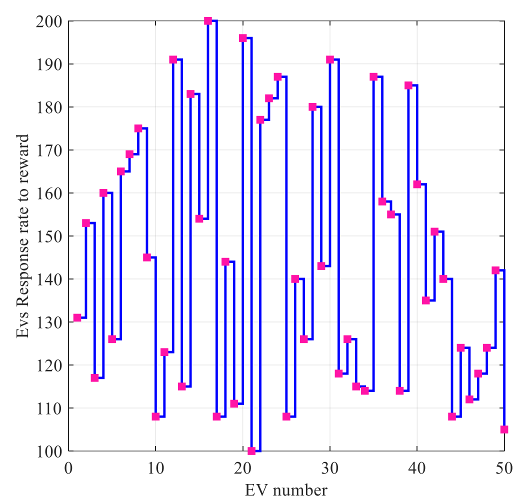

Fig. 11. Inverse slope of the performance curve for electric vehicles.

Fig. 12 illustrates the estimated hourly electrical energy demand ($xprex\_prexpre$) for the microgrid over a 24-hour period. The forecasted values range from a minimum of approximately 4.96 kWh in the early morning (about 2.16% of the daily peak) to a maximum of 229.43 kWh during the evening peak at hour 20 (100% reference). Demand remains below 20% of peak load for the first six hours of the day, then rises sharply between hours 7 and 9, reaching nearly 49% of the peak by mid-morning (111.51 kWh at hour 8). A secondary peak of 61.9% of maximum demand occurs at hour 14 (142.01 kWh) before the primary evening surge. This percentage-based load profile highlights the pronounced evening peak and midday consumption rise, providing the energy management system with essential insight for aligning distributed generation, scheduling electric vehicle charging, and minimizing costly grid imports during high-demand intervals.

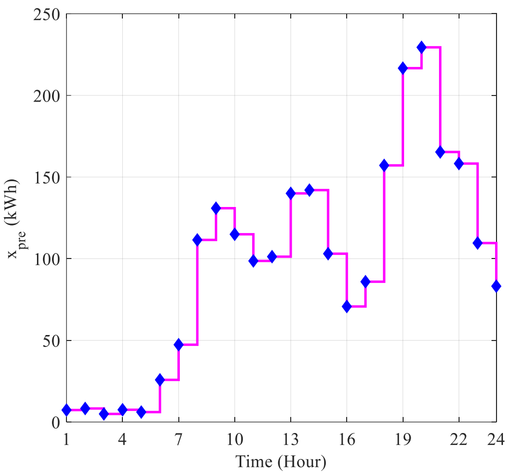

Fig. 12. Estimated Electrical Energy values.

The results in Fig. 13 (scenario S1) illustrate the 24-hour variation of electrical power production and demand within the studied microgrid. Load demand starts at around 45–55 kW during early morning hours, supplied mainly by the CHP unit (33–45 kW) and modest grid imports (7–12 kW). No EV or PV activity is observed at night. From 06:00 onward, demand rises sharply, reaching over 110 kW. EV charging becomes significant after 08:00, increasing from 39 kW to more than 100 kW by 10:00. This coincides with higher CHP output (up to 61 kW) and grid support exceeding 110 kW, while PV begins contributing around 49 kW. At midday (11:00–15:00), demand peaks near 190 kW, with EVs drawing 145 kW, CHP producing about 100 kW, and PV reaching 98 kW. Despite local generation, grid imports remain above 140 kW, showing the system's dependence on external supply. During the evening peak (20:00–21:00), load climbs again to 190–210 kW, EV demand stays above 100 kW, and CHP provides 82 kW. With PV absent, grid imports rise sharply, up to 232 kW, marking the highest reliance on the upstream network. Finally, at night (22:00–24:00), demand decreases to 120–130 kW, EV activity falls to ∼25 kW, and CHP contributes steadily near 95 kW, allowing grid imports to decline. In scenario S2, the daily load profile follows a similar pattern to S1, beginning at about 45–55 kW in the early morning and reaching over 190 kW in the evening. EV charging demand emerges around hour 08:00 at ∼39 kW, rising steadily to more than 140 kW by mid-afternoon. The CHP unit provides a stable contribution in the range of 36–86 kW across most hours, while PV generation peaks near 121 kW at midday before disappearing at sunset. Grid imports reach values exceeding 230 kW during the evening peak, compensating for the simultaneous high load and EV demand in the absence of PV. Compared to S1, the higher PV output in S2 reduces grid dependency slightly in daylight hours, but evening reliance on external supply remains dominant.

Scenario S3 represents the condition with the highest PV production among the three cases. While early-morning and night patterns resemble S1 and S2, the midday period shows stronger renewable support, with PV output exceeding 150 kW at its peak. CHP production remains steady between 39 and 85 kW, while EV demand again intensifies from 08:00 onward, reaching above 145 kW. Despite the stronger PV contribution, grid imports still rise above 220 kW in the evening hours (20:00–21:00), when PV is unavailable and both load and EV charging are high. Overall, S3 demonstrates that increased solar penetration alleviates grid purchases during daylight but cannot eliminate heavy evening dependency, highlighting the importance of coordinated EV scheduling and storage utilization.

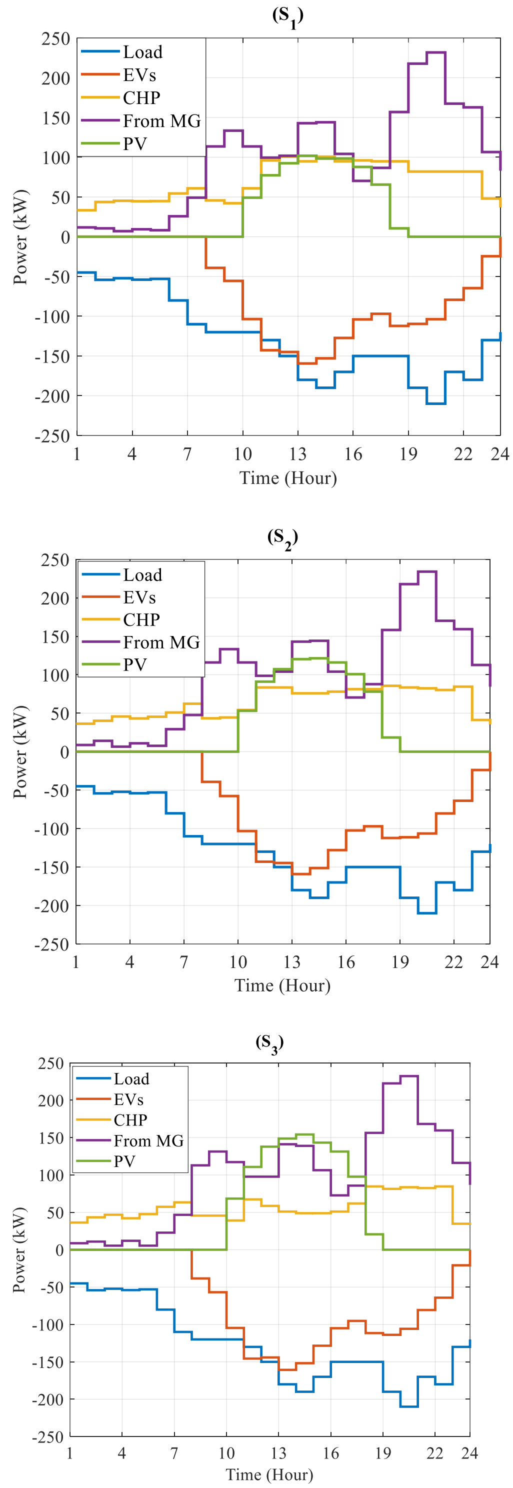

Fig. 13. Electrical power production values of units under different operating conditions.

The thermal power production of the microgrid under three operating scenarios is shown in Fig. 14. In scenario S1, thermal demand remains moderate (45–75 kW) during the first ten hours, supplied entirely by the CHP unit. A sharp increase occurs at 11:00, where demand reaches 132.7 kW. At this peak, CHP provides nearly 120 kW (≈90%), and the boiler supports 12.7 kW (≈10%). Between 12:00 and 14:00, the same trend continues, with CHP covering more than 92% of the thermal requirement. Afterward, demand gradually decreases to ∼100 kW by late evening, again fully met by CHP without boiler contribution. Thus, in S1, the CHP satisfies almost all thermal needs (≈96% of total energy), and the boiler plays only a marginal role during midday peaks. In S2, CHP participation is lower than in S1, leading to more significant boiler activity. At 10:00, demand is 75.2 kW, with CHP covering 64.5 kW (≈86%) and the boiler 10.7 kW (≈14%). The strongest divergence occurs between 11:00 and 14:00: at hour 11, the load is 132.7 kW, with CHP at 102.1 kW (≈77%) and the boiler at 30.6 kW (≈23%). A similar split is observed at 12:00 and 13:00, where the boiler consistently contributes 25–33% of demand. Later in the evening, CHP resumes dominance, covering nearly 100% of demand. Overall, S2 records a CHP share of about 80–82% and a boiler share of 18–20% over the full horizon. Scenario S3 demonstrates the heaviest reliance on the boiler. At 10:00, the load of 75.2 kW is split between CHP (48.4 kW, ≈64%) and boiler (26.8 kW, ≈36%). The midday peak at 11:00 is 132.7 kW, with CHP providing only 75.6 kW (≈57%) and the boiler 57.1 kW (≈43%). At 12:00 and 13:00, boiler shares exceed 50%, with CHP producing as low as 46–59 kW against boiler contributions of 65–69 kW. By hour 16, demand of 117.3 kW is supplied 57% by CHP and 43% by the boiler. In the evening hours, CHP regains full supply responsibility. On average, CHP supplies around 65–68% of total thermal demand, while the boiler contributes 32–35%.

The charging feasibility of representative electric vehicles is presented in Table 3. Two cases, EV5 and EV23, are examined over their actual connection window from 14:00 to 17:00, considering a nominal battery capacity of 90 kWh, a state-of-charge (SOC) cap of 95%, and a maximum charging limit of 8 kW per vehicle. These parameters determine the maximum achievable SOC increments within the available dwell times.

The results show that EV5 cannot reach the reported 82% SOC target within three hours at the 8 kW limit. Achieving this increase would require 26.1 kWh, whereas only 24 kWh can be stored during the dwell window. Under ideal conditions the feasible final SOC is 79.7%, which decreases to 78.3% at 95% charging efficiency. In contrast, EV23 can reach 80% SOC provided that its arrival SOC is no lower than 53–55%, a condition that is consistent with the observed fleet distribution where the average arrival SOC is 60.7%. This analysis highlights the importance of considering realistic technical limits in scheduling. Over the full 24-hour horizon, vehicle availability remains sparse, with occupancy ranging from 0 to 6 vehicles (0–12% of capacity) and a mean of 3.2 vehicles. This corresponds to an aggregated charging capacity of 0–48 kW, given the per-vehicle 8 kW limit. Within these limits, the optimization framework schedules EV charging flexibly, while the effects of solar irradiance manifest primarily in system-level dispatch decisions for the CHP unit, boiler, and grid exchange rather than in short per-vehicle charging profiles. It should also be noted that the 8 kW value is modeled as an upper bound on per-vehicle charging power, not a fixed charging rate. The optimizer is free to select any value between 0 and 8 kW depending on system conditions. Although a uniform cap was assumed for simplicity in this case study, the model can easily incorporate heterogeneous charging ratings (e.g., 3.3–11 kW) without altering the optimization framework.

3.3. Real-Time microgrid energy planning

In real-time energy planning, the microgrid operator must conduct precise planning based on real-time information. For real-time planning, data such as the capacity of photovoltaic generation, the number of electric vehicles in the parking lot, and the amount

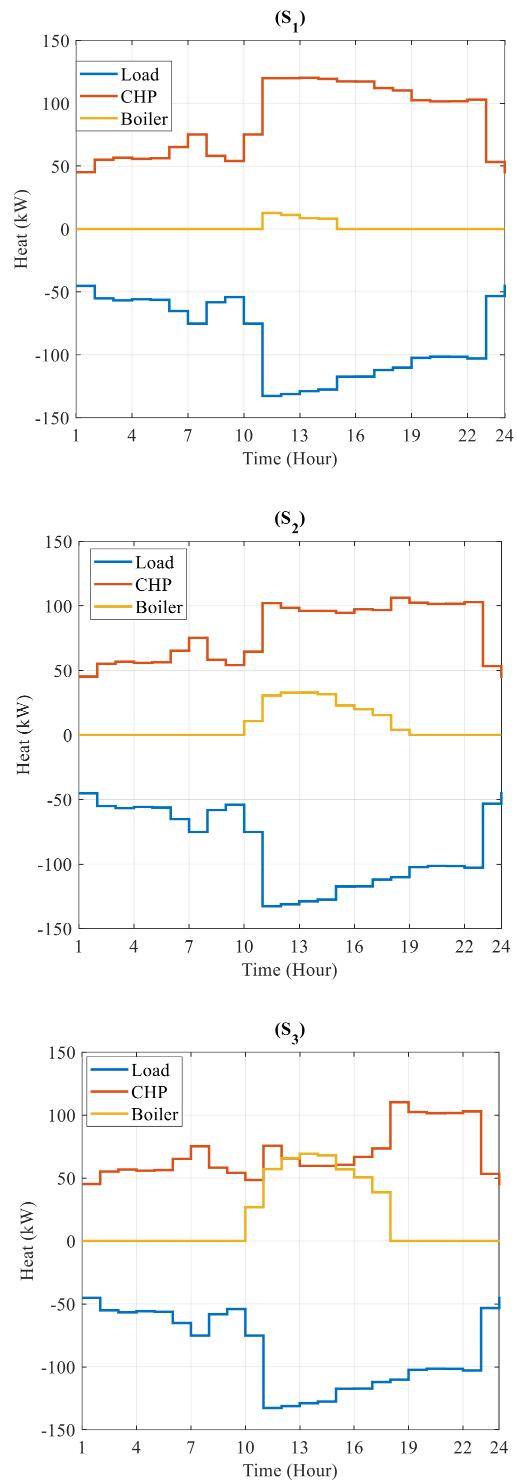

Fig. 14. Thermal power production of the microgrid under three operating scenarios.

of electric and thermal energy consumed in the microgrid must be determined. The exchange of electricity with the upstream grid must be optimized based on the estimated plans; otherwise, penalties for deviating from the predicted values must be paid. The microgrid operator should continuously review input and output data within specific time intervals and update precise operation plans using this information. If the energy production values of photovoltaic sources, the number of vehicles in the parking lot,

Table 3. Charging feasibility of EV5 and EV23 during the 14:00–17:00 window.

Vehicle	Connection window	Duration (h)	Arrival SOC (%)	Target SOC (%)	Energy required (kWh)	Maximum storable (kWh)	Feasible final SOC (ideal/95% η)	Feasibility
EV5	14:00–17:00	3	53.0	82.0	26.1	24.0	79.7/78.3	Not feasible
EV23	14:00–17:00	3	$\geq$ 53.3 (ideal) or $\geq$ 54.7 (95%)	80.0	$\leq$ 24.0	24.0	80.0 (if arrival SOC bound is met)	Feasible

the initial battery charge of the vehicles, or the electrical and thermal load in the microgrid differ from the estimated values, the pre-planned results will be invalid. The microgrid operator must devise new plans based on the actual values for a more accurate analysis of the proposed real-time planning method. To further analyze and scrutinize the performance of the proposed method in real-time planning, its performance was evaluated under two conditions: managing the charging of electric vehicles in the parking lot and unmanaged charging for the 2 PM time slot, which will be discussed in the following section.

- Optimized charging plan for electric vehicles in parking lots

In the first section, a simulation was conducted by introducing the capability of optimal management for charging electric vehicles in parking lots. Table 4 presents the results obtained from the simulation in this section.

Table 4. Simulation results with optimized charging management for electric vehicles at 2 PM.

Parameter	Scenario 1	Scenario 2	Scenario 3	Actual values
Photovoltaic Array	103	118	148	123.3
Number of Electric Vehicles	21	21	21	22
CHP Unit	97	86	47	100
Boiler	7.4	33	61	7.4
Purchased Electricity from the Grid	141	141	141	141

Considering the results recorded in Table 4, using the optimal management of electric vehicle charging in real-time planning, the profit obtained from optimal microgrid planning is $57.18/hour. This profit is higher than the estimated profit of $49.64/hour. Therefore, by employing optimal management of electric vehicle charging in parking lots in real-time planning, the operational profit of the microgrid increases. The number of electric vehicles present in the parking lot is determined to be 21, while the actual number of vehicles parked in the parking lot at this hour is 22. Given that the number of electric vehicles in the parking lot has changed, the production of the CHP unit should also be adjusted. Due to the change in the electric power output of the CHP unit, the amount of heat power produced in the microgrid also changes. In these circumstances, the microgrid operator must update the capacity of the boiler power production considering the heat demand in the microgrid and changes in the amount of heat produced by the CHP unit.

- Charging electric vehicles in parking without management

Regardless of optimal management of electric vehicle charging in parking lots, operators' efforts to reduce energy supply costs in the microgrid face serious challenges, and there is a possibility of unintentionally increasing the microgrid's consumption during peak hours. In this situation, increasing the number of electric vehicles in parking lots during peak consumption times may cause an increase in the microgrid's consumption, and the risk of electrical energy shortages and increased outages is also present. In this scenario, it is assumed that the microgrid operator cannot reduce the charging power of the vehicles, and each electric vehicle charges with its nominal power throughout all hours. The results of real-time planning in the new operating conditions at 2 PM are presented in Table 5.

After the energy operation, a profit of $42.35/hour is determined, which is lower compared to the conditions of optimal planning for charging electric cars in the parking lot. A penalty of $27.46 is specified to be paid under these conditions, whereas no penalty was paid in the planned conditions for charging the cars.

Table 5. Results without management of electric vehicle charging at 2 PM.

Parameter	Scenario 1	Scenario 2	Scenario 3	Actual Values
Photovoltaic Array	103	118	148	123.3
Number of Electric Vehicles	21	21	21	22
CHP Unit	97	86	47	100
Boiler	7.8	34.2	69	7.6
Purchased Electricity from the Grid	145	147	149	164

3.4. Scenario generation, validation, and sensitivity analysis

Photovoltaic (PV) output uncertainty in the day-ahead stage was modeled using three representative solar radiation scenarios derived from historical weather data for the study region. Hourly irradiance values were normalized to the installed PV capacity and fitted to a beta probability distribution with parameters $\alpha = 2$ and $\beta = 5$, selected through a method-of-moments fit to the observed distribution shape. This distribution captures the skewed nature of solar generation and reflects the higher likelihood of lower-to-moderate irradiance in the local climate. The three scenarios—low (S1), medium (S2), and high (S3)—were generated from quantiles of the fitted distribution, ensuring that they span the typical variability range. For the representative hour examined in detail, the PV outputs corresponding to S1, S2, and S3 were approximately 103 kW, 118 kW, and 148 kW, respectively, while the actual realized PV output was 123.3 kW, lying between S2 and S3. This confirms that the selected scenarios bracket the observed conditions and are not arbitrarily chosen.

The robustness of the optimization results was evaluated by applying the proposed scheduling approach under all three PV scenarios and comparing against an unmanaged charging baseline. In the managed case, the purchased energy from the grid at the representative hour remained constant at 141 kWh across S1–S3, indicating that the coordinated scheduling of PV, CHP, boiler, and incentive-based V2G effectively hedged PV variability. In contrast, the unmanaged case exhibited greater sensitivity: purchased grid energy rose from 145 kWh in S1 to 149 kWh in S3, with the actual condition requiring 164 kWh. This increased variability in the unmanaged case led to deviation penalties and reduced operational efficiency. The real-time optimized schedule achieved an operational profit of 57.18 USD/h, which is approximately 15.2% higher than the day-ahead estimate (49.64 USD/h) and 35.0% higher than the unmanaged case (42.35 USD/h). Moreover, compared with the unmanaged actual operation, the optimized approach reduced grid purchases by 23 kWh—about 14.0%—while avoiding penalties amounting to 27.46 USD. These results show that the selected scenarios, grounded in empirical data, provide a realistic range of solar generation conditions and that the proposed model delivers stable, high-performance outcomes across this range, thereby demonstrating robustness to renewable generation uncertainty.

3.5. Statistical validation of cost reduction with managed EV charging

The comparative performance of managed and unmanaged EV charging was evaluated through a stochastic Monte Carlo

Table 6. Summary of bus voltage and branch current statistics for the representative day (24 hours).

Metric	Managed (optimized)	Unmanaged (baseline)
Minimum bus voltage (p.u.)	0.965	0.945
Maximum bus voltage (p.u.)	1.046	1.051
Mean bus voltage (p.u.)	0.997	0.989
Standard deviation of bus voltages (p.u.)	0.014	0.019
Hours with $V < 0.95$ p.u. (count/% of 24 h)	0 (0 %)	3 (12.5 %)
Hours with $V > 1.05$ p.u. (count/% of 24 h)	0 (0 %)	0 (0 %)
Maximum branch loading (% of thermal rating)	78 %	103 %
Mean branch loading (% of thermal rating)	46 %	62 %
Hours with branch overload (> 100% rating)	0 (0 %)	3 (12.5 %)
Voltage Deviation Index (VDI, p.u.)	0.018	0.036

Table 7. Voltage stability and reliability indices for the representative day and Monte Carlo analysis.

Metric	Managed (optimized)	Unmanaged (baseline)
Average L-index (Kessel)	0.054	0.115
Maximum daily L-index	0.12	0.23
Voltage Stability Margin (VSM, %)	28 %	18 %
Probability of ≥ 1 hour/day with V or I violation	0 %	4 %
Expected Energy Not Supplied (EENS, kWh/day)	0.00	0.42

simulation framework to ensure robustness against variations in renewable generation, vehicle availability, and initial state-of-charge (SOC) levels. A total of 500 independent daily realizations were generated using the stochastic input models described in Section 2. Photovoltaic power was modeled using a beta distribution fitted to historical irradiance data, vehicle arrivals followed a normal distribution (mean 13.8 vehicles, standard deviation 4.6), and initial SOC values were sampled from the empirical distribution defined earlier. For each daily realization, the optimal scheduling model was solved twice: once with coordinated EV charging and vehicle-to-grid (V2G) participation, and once under unmanaged charging, where vehicles charged at a constant rated power whenever connected without coordination. All other system parameters, including time-of-use tariffs, combined heat and power (CHP) operation, and deviation penalties, were kept identical to isolate the impact of charging strategy.

The simulation results indicate that managed charging consistently achieved lower total daily operating costs. The average cost across all realizations was 1,178 USD for the managed strategy and 1,440 USD for the unmanaged case, corresponding to a mean cost reduction of 18.3%. The absolute mean saving was 262 USD per day with a 95% confidence interval of 243–281 USD. A paired statistical test confirmed that the observed difference is highly significant ($P < 10^{-6}$). The distribution of cost savings was tightly concentrated, with a median of 260 USD and an interquartile range of 58 USD, indicating that the benefit is not driven by outliers. A sensitivity analysis with varying EV penetration levels demonstrated a monotonic relationship between fleet size and cost reduction: 8.0% for 25 vehicles, 18.3% for 50 vehicles, and 27.1% for 75 vehicles. Similarly, adjusting the deviation penalty between 0.5 and 2.0 USD/kWh preserved the statistical significance of the savings, with larger penalties amplifying the benefit of managed charging.

3.6. Distribution-network voltage, current, reliability, and stability assessment

To complement the economic and operational results presented in the preceding sections, a technical evaluation of the distribution network's performance was carried out using the optimized schedules. For each hour, the active and reactive power set-points from the MILP optimization were applied to the network model. Bus voltage magnitudes and branch currents were recorded, along with the Voltage Deviation Index (VDI), defined as the mean absolute deviation of voltage from 1.0 p.u. across all buses and hours. Voltage stability was assessed using the Kessel L-index and a continuation power-flow to determine the Voltage Stability Margin (VSM) at the representative peak-load hour, expressed as the maximum uniform load increase before voltage collapse. Reliability indicators included the proportion of hours in which voltage or current limits were violated and the Expected Energy Not Supplied (EENS) under a simple load-shedding rule. The same 500 Monte Carlo realizations described earlier were used so that these technical results are directly comparable to the cost analysis.

Table 6 summarises voltage and current statistics for the representative day. With managed charging, the minimum daily voltage remained at 0.965 p.u., compared to 0.945 p.u. without coordination. The mean voltage increased from 0.989 p.u. to 0.997 p.u., and the VDI improved from 0.036 p.u. to 0.018 p.u. Voltage limit violations (V < 0.95 p.u.) occurred in 12.5% of hours in the unmanaged case but were eliminated entirely under coordinated charging. The maximum branch loading fell from 103% to 78% of thermal rating, removing all overload events.

Table 7 reports stability and reliability indices. The average L-index decreased from 0.115 to 0.054, while the maximum daily value dropped from 0.23 to 0.12. The VSM at the peak-load hour increased from 18% to 28%, indicating a ten-percentage-point improvement in the network's ability to accommodate additional demand before voltage collapse. Across the Monte Carlo scenarios, the probability of any voltage or current violation on a given day decreased from 4% to 0%, and EENS was reduced from 0.42 kWh/day to zero.

These results show that the proposed coordinated charging strategy not only reduces operating costs but also enhances electrical performance by maintaining bus voltages closer to nominal, reducing line loading, and improving overall voltage stability. The combination of higher VSM, lower L-index, and elimination of overloads demonstrates that the optimized schedules strengthen both the reliability and robustness of the distribution network, even under the variability of renewable generation and stochastic EV arrivals.

4. CONCLUSION

The presented framework demonstrates that combining endogenous incentive design for EV participation with joint electrical–thermal scheduling and a two-stage operational strategy yields substantial economic and operational advantages for microgrids. By unifying these elements within a single optimization problem, the approach not only addresses uncertainty in renewable generation and user behavior but also enhances energy efficiency, reduces reliance on external grid purchases, and strengthens system stability. The numerical evaluation confirms that such integrated decision-making can deliver double-digit percentage improvements in both profitability and energy utilization efficiency, positioning the method as a robust and scalable solution for future multi-energy microgrid deployments. In the case of optimal management of electric vehicle charging in the parking lot, the operator, in exchange for reducing the charging power of vehicles during certain predefined hours, offers discounts as rewards based on the performance levels of electric vehicles, which are paid to the owners of electric vehicles when they are present in the parking lot. In the proposed method, the operator treats the amount of reward that owners of electric vehicles receive as a decision variable. If the owner of an electric vehicle is not willing to participate in the charging management program, they do not receive any parking rewards. As a result, owners of electric vehicles, when parking in the parking lot, declare their willingness or unwillingness to participate in microgrid charging management programs and, if willing, provide information on the performance of their electric vehicles.

While the proposed model demonstrates strong potential in improving operational efficiency and reliability of integrated energy systems, several limitations should be acknowledged. The formulation relies on simplified representations of certain technical components, such as linearized device models and a simplified treatment of battery degradation, which may not fully capture the complexities of real-world operation. Uncertainty is addressed for a limited set of variables, and other potential sources of variability, including dynamic load patterns, market fluctuations, and communication delays, are not explicitly modeled. Furthermore, the model assumes ideal communication and control infrastructures without considering cyber-security risks or partial observability. Future research should address these aspects by incorporating more detailed component models, broader uncertainty representations, diverse case studies, and advanced optimization approaches to improve scalability. In addition, integrating realistic behavioral models for energy users and exploring field demonstrations would enhance the practical applicability and robustness of the proposed framework.

ACKNOWLEDGEMENT

The authors acknowledge the use of artificial intelligence tools (e.g., ChatGPT by OpenAI) for language editing and clarity improvement during the preparation of this manuscript. The authors are fully responsible for the scientific content, analysis, and conclusions.

REFERENCES

[1] M. Megrini, A. Gaga, and Y. Mehdaoui, "Review of electric vehicle traction motors, control systems, and various implementation cards," *J. Oper. Autom. Power Eng.*, vol. 13, no. 3, pp. 238–247, 2025.

[2] E. Littwitz and O. Ayalon, "Feasibility analysis of storage and renewable energy ancillary services for grid operations," *Energies*, vol. 18, no. 11, p. 2836, 2025.

[3] S. Mohammad and A. Ghasemi-Marzbali, "Fast-charging station for electric vehicles, challenges and issues: A comprehensive review," *J. Energy Storage*, vol. 49, p. 104136, 2022.

[4] M. A. El-Meligy, M. Sharaf, K. A. Alnowibet, and A. E. Abdelgawad, "A second-order cone programming-based microgrid bidding strategy considering real-time market price correlation," *Electr. Eng.*, pp. 1–14, 2025.

[5] M. Farhoumandi, S. Bahramirad, M. Shahidehpour, and A. Alabdulwahab, "Blockchain for peer-to-peer energy trading in electric vehicle charging stations with constrained power distribution and urban transportation networks," *Energy Internet*, vol. 2, no. 1, pp. 28–44, 2025.

[6] S. Chinnaperumal, S. K. Raju, A. H. Alharbi, S. Kannan, D. S. Khafaga, M. Periyasamy, M. M. Eid, and E.-S. M. El-Kenawy, "Decentralized energy optimization using blockchain with battery storage and electric vehicle networks," *Sci. Rep.*, vol. 15, no. 1, p. 5940, 2025.

[7] S. Kumar, K. C. Ramaswamy, S. R. Mathiyalagan, J. Giri, and M. Kanan, "An efficient battery management system for electric vehicles using iot and blockchain," *Results Eng.*, p. 106284, 2025.

[8] M. C. Kintner-Meyer, S. Sridhar, C. Holland, A. Singhal, K. E. Wolf, C. J. Larimer, C. R. McGrath, A. A. Bleeker, and R. E. Murali, "Electric vehicles at scale–phase II–distribution systems analysis," Tech. Rep. PNNL-32460, Pacific Northwest National Lab.(PNNL), Richland, WA, USA, 2022.

[9] S. Gupta, A. Maulik, D. Das, and A. Singh, "Coordinated stochastic optimal energy management of grid-connected microgrids considering demand response, plug-in hybrid electric vehicles, and smart transformers," *Renew. Sustain. Energy Rev.*, vol. 155, p. 111861, 2022.

[10] Z. Yang, F. Yang, H. Min, H. Tian, W. Hu, J. Liu, and N. Eghbalian, "Energy management programming to reduce distribution network operating costs in the presence of electric vehicles and renewable energy sources," *Energy*, vol. 263, p. 125695, 2023.

[11] S. Rahman, I. A. Khan, A. A. Khan, A. Mallik, and M. F. Nadeem, "Comprehensive review and impact analysis of integrating projected electric vehicle charging load to the existing low voltage distribution system," *Renew. Sustain. Energy Rev.*, vol. 153, p. 111756, 2022.

[12] K. Bakht, S. A. R. Kashif, M. S. Fakhar, I. A. Khan, and G. Abbas, "Accelerated particle swarm optimization algorithms coupled with analysis of variance for intelligent charging of plug-in hybrid electric vehicles," *Energies*, vol. 16, no. 7, p. 3210, 2023.

[13] J. Hu, D. Liu, C. Du, F. Yan, and C. Lv, "Intelligent energy management strategy of hybrid energy storage system for electric vehicle based on driving pattern recognition," *Energy*, vol. 198, p. 117298, 2020.

[14] H. F. Gharibeh, A. S. Yazdankhah, and M. R. Azizian, "Energy management of fuel cell electric vehicles based on working condition identification of energy storage systems, vehicle driving performance, and dynamic power factor," *J. Energy Storage*, vol. 31, p. 101760, 2020.

[15] B. Xu, D. Rathod, D. Zhang, A. Yebi, X. Zhang, X. Li, and Z. Filipi, "Parametric study on reinforcement learning optimized energy management strategy for a hybrid electric vehicle," *Appl. Energy*, vol. 259, p. 114200, 2020.

[16] X. Hou, J. Wang, T. Huang, T. Wang, and P. Wang, "Smart home energy management optimization method considering energy storage and electric vehicle," *IEEE Access*, vol. 7, pp. 144010–144020, 2019.

[17] C. Yang, M. Zha, W. Wang, K. Liu, and C. Xiang, "Efficient energy management strategy for hybrid electric vehicles and plug-in hybrid electric vehicles: review and recent advances under intelligent transportation system," *IET Intell. Transp. Syst.*, vol. 14, no. 7, pp. 702–711, 2020.

[18] A. M. Fernandez, M. Kandidayeni, L. Boulon, and H. Chaoui, "An adaptive state machine based energy management strategy for a multi-stack fuel cell hybrid electric vehicle," *IEEE Trans. Veh. Technol.*, vol. 69, no. 1, pp. 220–234, 2019.

[19] H. Dang, Y. Han, Y. Hao, P. Sun, and Z. Chen, "Energy management optimization of plug-in hybrid electric vehicle in microgrid with information-physics-traffic coupling," *Electr. Power Syst. Res.*, vol. 238, p. 111194, 2025.
[20] A. B. Etemesi, T. F. Megahed, H. Kanaya, and D. E. A. Mansour, "IoT based energy management of smart microgrid considering electric vehicle integration," *Energy*, p. 136405, 2025.
[21] K. Kioumarsi and A. Bolurian, "Optimal energy management for electric vehicle charging parking lots considering renewable energy resources and accurate battery characteristic modeling," *J. Energy Storage*, vol. 107, p. 114914, 2025.
[22] T. Hai, N. S. S. Singh, and F. Jamal, "Energy management of a microgrid with integration of renewable energy sources considering energy storage systems with electricity price," *J. Energy Storage*, vol. 110, p. 115191, 2025.
[23] L. Wang, Q. Sun, X. Wang, T. Shi, X. Yang, and H. Xu, "Low carbon planning of flexible distribution network considering orderly charging and discharging of electric vehicles," *Electr. Power Syst. Res.*, vol. 244, p. 111546, 2025.
[24] S. Abdullah-Al-Nahid, T. A. Khan, M. A. Taseen, T. Jamal, and T. Aziz, "A novel consumer-friendly electric vehicle charging scheme with vehicle-to-grid provision supported by genetic algorithm based optimization," *J. Energy Storage*, vol. 50, p. 104655, 2022.
[25] X. Hu, C. Zou, X. Tang, T. Liu, and L. Hu, "Cost-optimal energy management of hybrid electric vehicles using fuel cell and battery health-aware predictive control," *IEEE Trans. Power Electron.*, vol. 35, no. 1, pp. 382–392, 2019.
[26] M. A. Mohamed, H. M. Abdullah, M. A. El-Meligy, M. Sharaf, A. T. Soliman, and A. Hajjiah, "A novel fuzzy cloud stochastic framework for energy management of renewable microgrids based on maximum deployment of electric vehicles," *Int. J. Electr. Power Energy Syst.*, vol. 129, p. 106845, 2021.
[27] Y. Zhou, H. Li, A. Ravey, and M.-C. Péra, "An integrated predictive energy management for light-duty range-extended plug-in fuel cell electric vehicle," *J. Power Sources*, vol. 451, p. 227780, 2020.
[28] M. A. Babajani-Chari and A. Ghasemi-Marzbali, "Stochastic optimization of a multi-carrier energy system with the participation of renewable energy sources and integrated demand response programs," *Sci. Iran.*, 2025.
[29] S. A. Mansouri, A. Ahmarinejad, E. Nematbakhsh, M. S. Javadi, A. R. Jordehi, and J. P. Catalao, "Energy management in microgrids including smart homes: A multi-objective approach," *Sustain. Cities Soc.*, p. 102852, 2021.